Front- and Back-illuminated X-ray CCD Performance in Low- and High-Earth Orbit: Performance trends of Suzaku XIS and Chandra ACIS Detectors

Beverly LaMarr[a], Catherine Grant[a], Steve Kissel[a], Gregory Prigozhin[a], Mark Bautz[a], Takeshi Go Tsuru[b], Hiroshi Tsunemi[c], Tadayasu Dotani[d], Kiyoshi Hayashida[c], and Hironori Matsumoto[b]

[a]MIT Kavli Institute for Astrophysics and Space Research, Massachusetts Institute of Technology, Cambridge MA, USA;
[b]Department of Physics, Kyoto University, Kyoto, Japan;
[c]Department of Earth and Space Science, Osaka University, Osaka, Japan;
[d]Institute of Space and Astronautical Science, Japan Aerospace Exploration Agency, Kagawa, Japan

ABSTRACT

Since the launch of the Suzaku X-ray astronomy satellite into low- earth orbit in July, 2005, the performance of the CCD detectors in the X-ray Imaging Spectrometer (XIS) detectors have slowly degraded, as expected, due to accumulating radiation damage. We compare the evolution of front- and back-illuminated XIS CCDs with one another and with that of very similar detectors installed in the ACIS instrument aboard the Chandra X-ray Observatory, which is in a much higher orbit than Suzaku. We attempt to identify effects of the differing radiation environments as well as those arising from structural differences between the two types of detector.

Keywords: X-ray, CCD, radiation damage, ACIS, XIS, Chandra, Suzaku

1. INTRODUCTION

The Chandra X-ray Observatory,[1] the third of NASA's great observatories in space was launched on July 23, 1999. Suzaku,[2] Japan's fifth X-ray Astronomy satellite, was launched on July 10, 2005. Both are equipped with science instruments featuring charge coupled devices (CCDs) provided by MIT Lincoln Laboratory. The Advanced CCD Imaging Spectrometer (ACIS) is on-board Chandra and the X-ray Imaging Spectrometer (XIS) is on Suzaku. While there are a few differences between the devices, the similarities allow us to compare the effects of their respective orbits and operating conditions on their evolving spectral performance.

2. THE FOCAL PLANES

The ACIS focal plane consists of ten CCID17 devices, eight of which are Front Illuminated (FI), two of which are Back Illuminated (BI). The four XIS devices are CCID41s, three FIs and one BI.[3] One of the FI devices (XIS2) failed, probably due to a micrometorite strike, seventeen months after launch.

The characteristics of the MIT Lincoln Laboratory CCDs are described in Table 1.[4,5]

The devices are very similar with the primary difference being the addition of charge injection capabilities in the CCID41.

Both are equipped with on-board calibration sources. For ACIS to view its calibration source, it is moved out of the focus of the telescope. The advantage is that the entire CCDs are nearly uniformly illuminated. The disadvantage is that the calibration source is only observed once an orbit (about every 2.5 days). Each of the XIS sensors is constantly illuminated in the two corners farthest from the framestore. Here the advantage is

Send correspondence to B.L.
B.L.: E-mail: fergason@space.mit.edu, Telephone: 617 258 8153

Space Telescopes and Instrumentation 2008: Ultraviolet to Gamma Ray, edited by Martin J. L. Turner, Kathryn A. Flanagan, Proc. of SPIE Vol. 7011, 70112C, (2008) · 0277-786X/08/$18 · doi: 10.1117/12.788168

	ACIS	XIS
Model	CCID17	CCID41
Format	1026 rows × 1024 pixels/row (imaging area)	same
Architecture	3-phase, frame-transfer, four parallel output nodes	same
Illumination Geometry	8 front-illuminated (FI) & 2 back-illuminated (BI)	2 FI & 1 BI
Charge Injection Capable	no	yes
Pixel Size	$24 \times 24\mu$m	same
Readout noise	2-3 e^- RMS at 400 kpix s^{-1}	$< 2.5e^-$ RMS at 41 kpix s^{-1}
Depletion Depth	FI: 64 - 76 μm; BI: 30 - 40 μm	FI: 60 - 65 μm; BI: 40 - 45 μm
Operating Temperature	-120C via Radiative Cooling	-90C via Peltier cooler

Table 1. Characteristics of MIT Lincoln Laboratory CCDs for ACIS and XIS

the constant availability of calibration data, with the disadvantage that the illumination pattern is extremely nonuniform.

In both cases, the primary calibration source is radioactive decay of ^{55}Fe with the main peak at Mn-Kα (5.9 keV). The calibration source for ACIS also includes titanium and aluminium targets giving the additional lines of Ti-Kα (4.5 keV) and Al-Kα (1.5 keV).

Traditionally the charge transfer inefficiency (CTI) is used as the measure of radiation damage for CCDs. CTI is defined by the slope and intercept of a line fit to the measured pulse height as a function of distance to the readout. This number is not used in this paper because the nonuniformity of the calibration sources on-board XIS does not allow the value to be calculated. Instead the location of the main spectral peaks far from the readout normalized to the beginning of the missions is used. This method does not allow us to separate changes in the gain of the electronics from changes in CTI.

Figures 1 and 2 show the change in the location of the 5.9keV peak as a function of time for ACIS and XIS respectively. Only data from the top 200 rows of the CCDs (those furthest from the readout) are considered. The data sets have been filtered to include only points at the nominal operating temperatures for the focal planes; -120C for ACIS and -90C for XIS. Only full frame, timed exposure clocking mode data at the nominal exposure times of 3.2 seconds for ACIS and 8 seconds for XIS are included. Each point for ACIS includes one science run taken before or after radiation belt passage while the instrument is exposed to its calibration source. Each data point for XIS includes data for a single day. The gain change axis for each sets of figures is the same, but the time axis is different. The ACIS plots include data from early 2000 (when the focal plane temperature was lowered to the current value of -120C) to Spring 2008. The XIS plots span Summer of 2005 (just after launch) to Spring of 2008.

For ACIS, where the CCDs are uniformly illuminated, CTI and gain can be separated using data closest to the readout. Two of the ACIS devices, i0 and i2, do have gain changes that are clearly not due to CTI. Data from those devices are not included here.

The ACIS FI peaks, shown in Figure 1 do not decrease linearly with time. This is due to the effects described in Section 3. From the end of 2000 through mid 2003 the background rates were fairly stable (see Figure 4.) The results of a linear fit to the peak changes as a function of time during that period are tabulated in Table 2. The Mn Kβ peaks are not included here because they are not well resolved on the ACIS FI devices.

The XIS peaks are shown in Figure 2. The charge injection (SCI) feature was not used for regular operations until late in 2006. Points early in the mission are with charge injection turned off, and the second set of points on each plot are for charge injection turned on. We see no changes in the calibration peaks of the XIS devices that suggest changes in the gain of the electronics.

The results of a linear fit to changes in the peak for data with and with out charge injection at both the Mn-Kα and Mn-Kβ peaks are presented in Table 3.

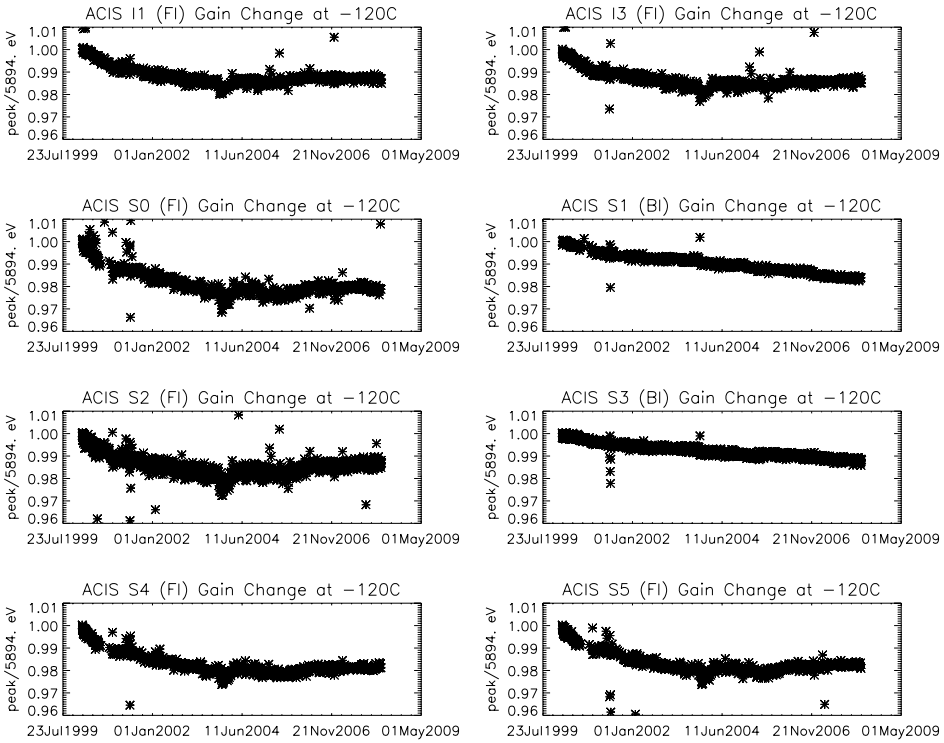

Figure 1. Gain Change for ACIS. The normalized peak of the calibration source line at 5.9 keV measured in the top 200 rows of the image area. Only data with a focal plane temperature of -119C and below are included.

CCD	Change in Peak Location Mn Kα (percent/year)
i1	-0.345 +/- 0.001
i3	-0.349 +/- 0.001
s0	-0.535 +/- 0.002
s1 (BI)	-0.208 +/- 0.001
s2	-0.405 +/- 0.001
s3 (BI)	-0.168 +/- 0.000
s4	-0.443 +/- 0.001
s5	-0.446 +/- 0.001

Table 2. ACIS Change in Peak Location

	Change in Peak Location (percent/year)			
	SCI off		SCI on	
	Mn Kα	Mn Kβ	Mn Kα	Mn Kβ
XIS0	-1.804 +/- 0.003	-1.733 +/- 0.007	-0.410 +/- 0.002	-0.414 +/- 0.004
XIS1 (BI)	-1.966 +/- 0.004	-1.868 +/- 0.009	-0.865 +/- 0.003	-0.888 +/- 0.007
XIS2	-1.733 +/- 0.002	-1.785 +/- 0.004	N/A	N/A
XIS3	-1.785 +/- 0.004	-1.726 +/- 0.007	-0.379 +/- 0.002	-0.380 +/- 0.005

Table 3. XIS Change in Peak Location

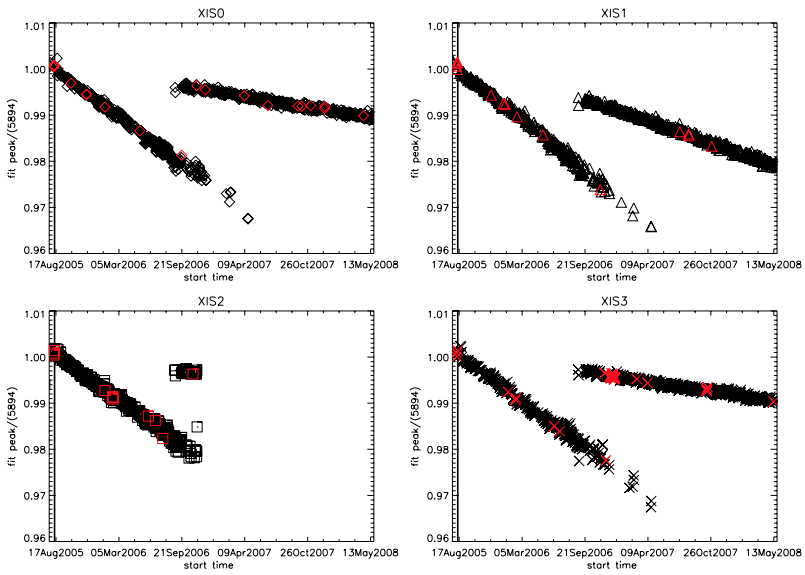

Figure 2. Change in the Location of the Manganese Kα Peak for XIS as a Function of Time.

3. DIFFERENCES IN ENVIRONMENT

Chandra's initial orbit had a perigee of 10,000 km and and apogee of 140,000 km with an initial inclination of 28.5deg. This orbit brings the satellite into the Earth's radiation belts. During several orbits in the fall of 1999, ACIS was in the focus of the telescope through the radiation belts. The majority of the radiation damage to the ACIS front illuminated (FI) devices was accumulated during these passes as low energy protons were focused by the high resolution mirror assembly.[6]

The measured ACIS instrument background is shown in Figure 3. The solid line is for an FI (s2) and the dashed line is for a BI (s3). These spectra, included in the Chandra calibration database, were taken with ACIS out of focus of the telescope but not under the calibration source in December of 2000.

Due to Chandra's orbit, the particle rate is very dependent on the solar activity. A measure of the background is the high energy reject rate (events above 3750 adu or around 16keV per exposure) for s3 which is shown in Figure 4. Since its lowest point, just after solar maximum, this value has doubled. It is expected to slowly return to lower levels now that solar minimum has passed.

Suzaku's orbit is nearly circular at 570 km and an inclination of 31deg. The particle background rate in this orbit is much lower. Background spectra from the Suzaku calibration database are plotted in Figure 5. These spectra are created using times when the XIS is looking at the dark earth. The solid line is an FI (xis0). The dashed line is the BI (xis1).

The background rate on Suzaku varies during its orbit as the Magnetic Cut Off Rigidity (COR) changes. Figure 6 shows the number of events with pulse heights greater than 3750 adu for XIS1, the BI device on Suzaku, as a function of COR. Each day brings XIS through a wide range of COR values so the effect is averaged out during normal data processing. The Suzaku orbit does pass through the South Atlantic Anomaly (SAA) four or five times each day. Data are not available for these passes because the CCDs are powered down to minimize damage.

4. SACRIFICIAL CHARGE EFFECTS

The performance of CCDs degrades as radiation causes an increase in the number of traps. Some of the charge associated with each x-ray is lost to a trap as it is transfered through during the readout. However, if the trap is already full of charge when the packet is transfered through, there is little to no loss. This sacrificial charge can have a noticeable effect on the gain of a device with measurable CTI.

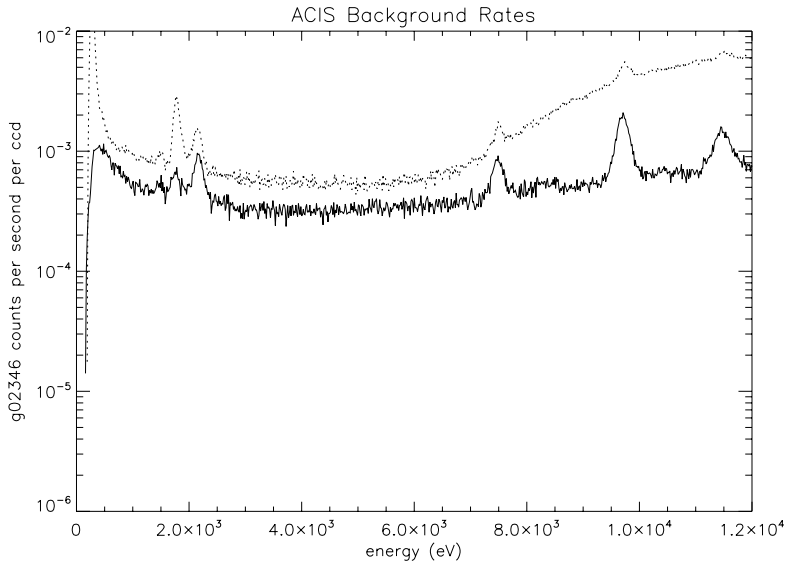

Figure 3. ACIS background spectrum. The solid line is s2 (FI). The dashed line is s3 (BI). These data were taken while ACIS was stowed; neither in the telescope focus nor under its calibration source. Note that the scales are identical to those in Figure 5.

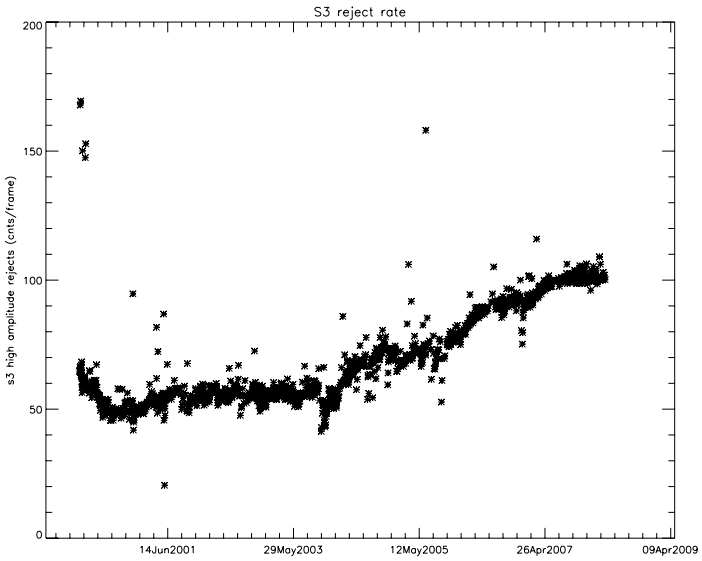

Figure 4. High Energy Reject Rate for ACIS S3 (BI). This value is a measure of the background rate.

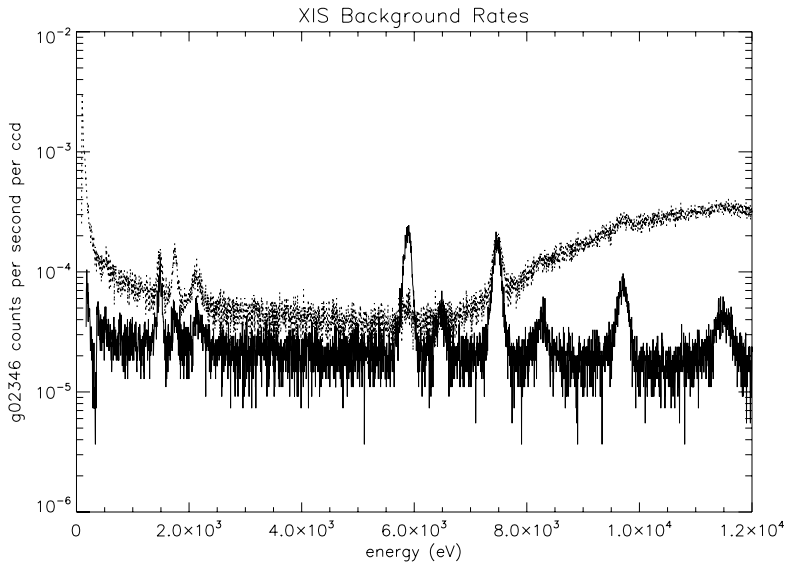

Figure 5. XIS background spectrum. The solid line is xis0 (FI). The dashed line is xis1 (BI). These spectra were taken when Suzaku is viewing the dark Earth. Note that the scales are identical to those in Figure 3.

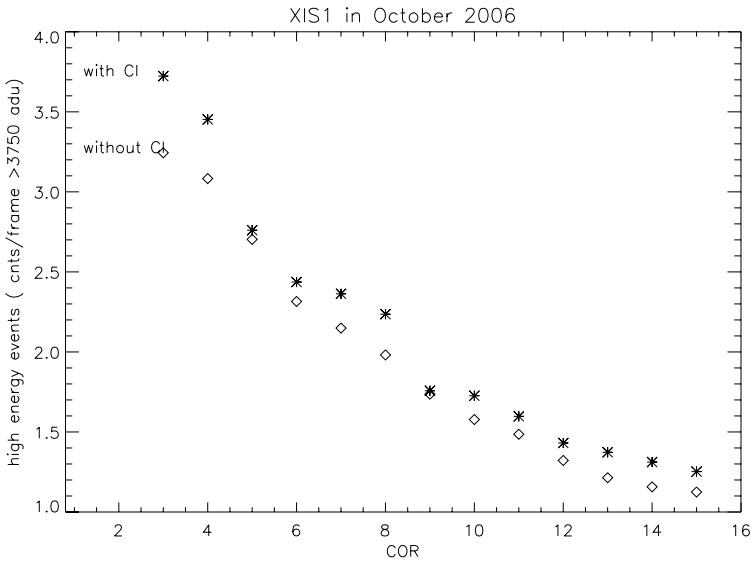

Figure 6. Change in the high energy count rate in XIS1 as a Function of Cut Off Rigidity. Diamonds represent data with the spaced row charge injection (SCI) turned on. asterisk are for data with SCI turned off.

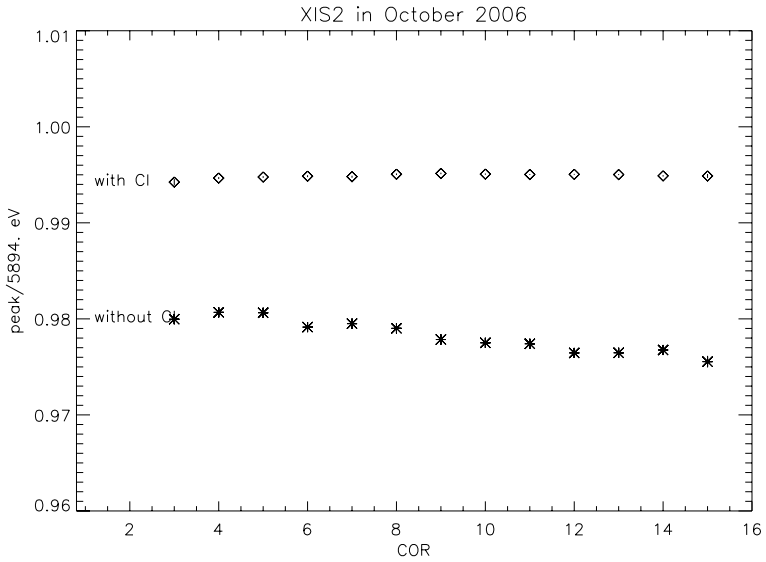

Figure 7. Change in the Location of the Manganese Kα Peak for XIS2 as a Function of Cut Off Rigidity. Diamonds represent data with the spaced row charge injection (SCI) turned on. Asterisk are for data with SCI turned off.

ACIS background is a significant source of sacrificial charge and so a contributor to the measured CTI and gain for the instrument. Cosmic rays that hit the FI devices bloom, adding significant sacrificial charge to each frame.

The effect of background variations on ACIS CTI are well known .[7]

The XIS background varies as during the orbit. The COR is a measure of this. When the space row charge injection is turned off, the additional background from the low COR times acts as sacrificial charge and increases the location of the peak while decreasing the FWHM (see Figures 7 and 8.) Because the level of sacrificial charge imparted by the SCI is much greater than that given by the background, the COR has little effect on the peak and width while it is turned on.

The most striking example of the effectiveness of sacrificial charge is the sudden jump in peak locations when the spaced row charge injection was turned on for regular operations for the XIS devices. In Figure 2 the location of the peak for each of the XIS devices is plotted as a function of time. During the second half of 2006 data was regularly taken both with SCI on and with SCI off. The locations of the peaks with SCI on were nearly at the beginning of mission values.

The difference between FI and BI devices is significant for the ACIS devices. Because the initial radiation damage was due to low energy protons the BIs were not affected. The overall performance degradation due to radiation damage is much higher for the FIs. The higher cosmic ray background for Chandra also has a bigger impact on the FI devices because the large charge blooms that result fill more traps to provide more sacrificial charge. This is especially obvious in Figure 9.

On Suzaku the differences between FI and BI are not as pronounced. There is not significant damage due to low energy protons on the XIS devices. The cosmic ray background is much lower and the use of charge injection has made it irrelevant.

5. DISCUSSION AND SUMMARY

The rates of change of gain for ACIS and XIS are compared in Figure 10. All devices show declining gain due to accumulating radiation damage. Care must be taken in comparing these rates because detector operating temperature, readout rates, and radiation environments for the two instorments differ. A rough estimate derived

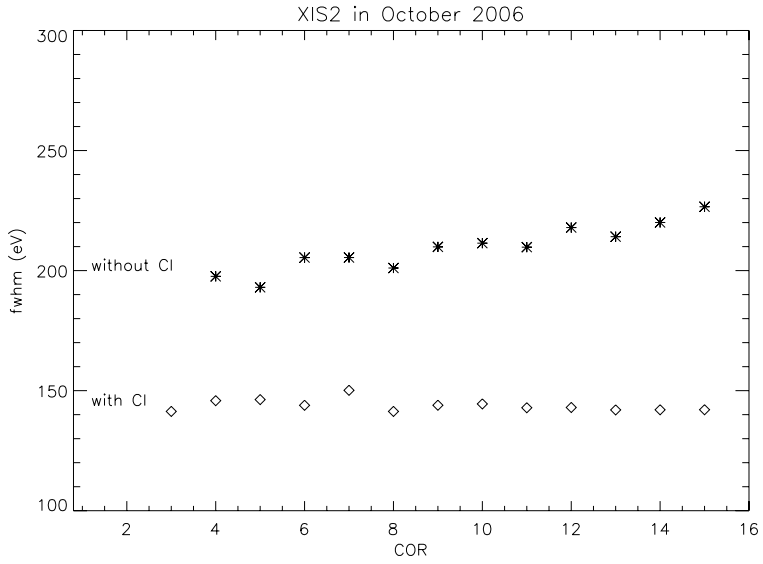

Figure 8. Change in the width of the Manganese Kα Peak for XIS2 as a Function of Cut Off Rigidity. Diamonds represent data with the spaced row charge injection (SCI) turned on. Asterisk are for data with SCI turned off.

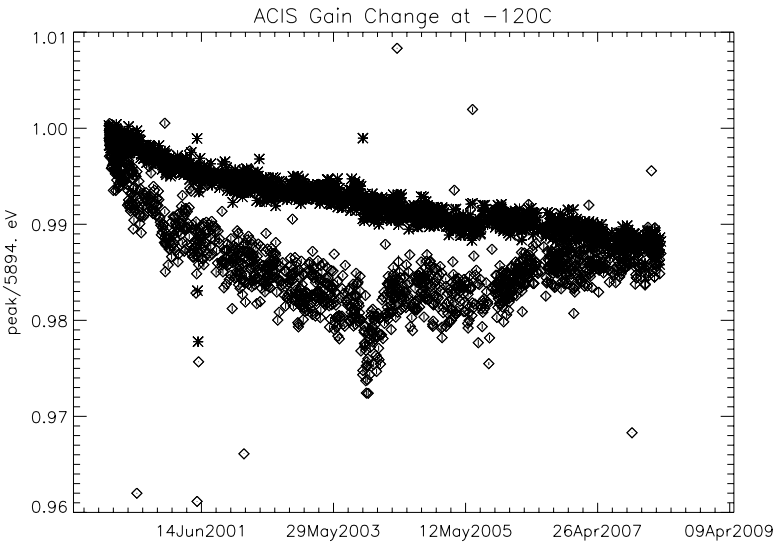

Figure 9. Gain Change for ACIS. The normalized peak of the calibration source line at 5.9 keV measured in the top 200 rows of the image area. Asterisk are for ACIS S3 (BI) and diamonds are for ACIS S2 (FI). Only data with a focal plane temperature of -119C and below are included.

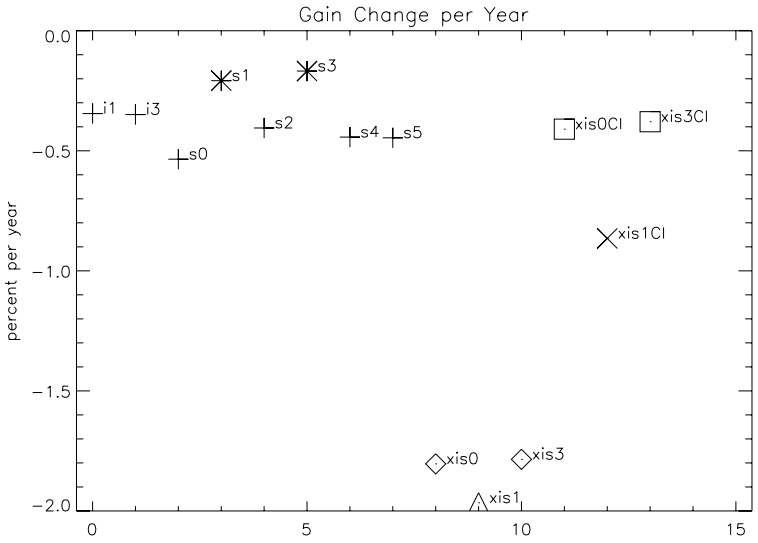

Figure 10. Percentage Gain Change Per Year for ACIS and XIS. Plus signs indicate ACIS FI devices, asterisks for ACIS BI devices, diamonds for XIS FI without SCI, triangle for XIS BI without SCI, square for XIS FI with SCI, X for XIS BI with SCI

from ESA's SPENVIS * suggests that the non-ionizing radiation does is about a factor of two lower for Chandra ACIS than for Suzaku XIS.

Figure 10 shows that the ACIS FI devices are changing faster than the ACIS BI devices. Presumably this difference is the result of damage from very soft (E<0.5 MeV) protons encountered in Chandra's high orbit.

The relatively rapid degradation of the XIS detectors without charge injection reflects the combined effects of the higher radiation dose, higher detector operating temperature, and much lower sacrificial charge background of the XIS. The XIS charge injection compensates for all of these factors, however. Thus charge injection is especially beneficial for CCD instruments in inclined, low-earth orbits.

The XIS BI does not improve as much with SCI only because the commanded amount of charge being injected is lower. This is not a constraint in the hardware, but an operational choice at this time.

ACKNOWLEDGMENTS

This work was supported by NASA contracts NAS8-37716 and NNG-05GM92G and by funding from the Institute of Space and Astronautical Science, Japan Aerospace Exploration Agency.

REFERENCES

[1] Weisskopf, M. C., Aldcroft, T. L., Bautz, M., Cameron, R. A., Dewey, D., Drake, J. J., Grant, C. E., Marshall, H. L., and Murray, S. S., "An Overview of the Performance of the Chandra X-ray Observatory," *Experimental Astronomy* **16**, 1–68 (Aug. 2003).

[2] Inoue, H., "Astro-E2 mission: the third X-ray observatory in the 21st century," in [*X-Ray and Gamma-Ray Telescopes and Instruments for Astronomy. Edited by Joachim E. Truemper, Harvey D. Tananbaum. Proceedings of the SPIE, Volume 4851, pp. 289-292 (2003).*], Truemper, J. E. and Tananbaum, H. D., eds., 289–292 (Mar. 2003).

[3] Lesser, M. P. and Iyer, V., "Enhancing back-illuminated performance of astronomical CCDs," in [*Proc. SPIE Vol. 3355, p. 446-456, Optical Astronomical Instrumentation, Sandro D'Odorico; Ed.*], D'Odorico, S., ed., 446–456 (July 1998).

*http://www.spenvis.oma.be

[4] Pivovaroff, M., Kissel, S., Bautz, M., Prigozhin, G., Isobe, T., and Gregory, J. A., "Flight x-ray ccd selection for the axaf ccd imaging spectrometer," *Proc. SPIE* **2080**, 182 (1996).

[5] Bautz, M. W., Kissel, S. E., Prigozhin, G. Y., LaMarr, B., Burke, B. E., and Gregory, J. A., "Progress in x-ray CCD sensor performance for the Astro-E2 X-ray imaging spectrometer," in [*Optical and Infrared Detectors for Astronomy. Edited by Garnett, James D.; Beletic, James W. Proceedings of the SPIE, Volume 5501, pp. 111-122 (2004).*], Holland, A. D., ed., 111–122 (Sept. 2004).

[6] Prigozhin, G. Y., Kissel, S. E., Bautz, M. W., Grant, C., LaMarr, B., Foster, R. F., and Ricker, G. R., "Characterization of the radiation damage in the Chandra x-ray CCDs," in [*Proc. SPIE Vol. 4140, p. 123-134, X-Ray and Gamma-Ray Instrumentation for Astronomy XI, Kathryn A. Flanagan; Oswald H. Siegmund; Eds.*], Flanagan, K. A. and Siegmund, O. H., eds., *Presented at the Society of Photo-Optical Instrumentation Engineers (SPIE) Conference* **4140**, 123–134 (Dec. 2000).

[7] Grant, C. E., Bautz, M. W., Kissel, S. M., LaMarr, B., and Prigozhin, G. Y., "Long-term trends in radiation damage of Chandra x-ray CCDs," in [*UV, X-Ray, and Gamma-Ray Space Instrumentation for Astronomy XIV. Edited by Siegmund, Oswald H. W. Proceedings of the SPIE, Volume 5898, pp. 201-211 (2005).*], Siegmund, O. H. W., ed., 201–211 (Aug. 2005).